Directional torsion and temperature discrimination based on a multicore fiber with a helical structure

Zhang, Hailiang; Wu, Zhifang; Shum, Perry Ping; Shao, Xuguang; Wang, Ruoxu; Dinh, Xuan Quyen; Fu, Songnian; Tong, Weijun; Tang, Ming

2018

Zhang, H., Wu, Z., Shum, P. P., Shao, X., Wang, R., Dinh, X. Q., . . . Tang, M. (2018). Directional torsion and temperature discrimination based on a multicore fiber with a helical structure. Optics Express, 26(1), 544-. doi:10.1364/OE.26.000544

https://hdl.handle.net/10356/83142

https://doi.org/10.1364/OE.26.000544

Research Article | Vol. 26, No. 1 | 8 Jan 2018 | OPTICS EXPRESS 544
Optics EXPRESS

Directional torsion and temperature discrimination based on a multicore fiber with a helical structure

HAILIANG ZHANG,[1,2] ZHIFANG WU,[1,3,7] PERRY PING SHUM,[1,2,8] XUGUANG SHAO,[1] RUOXU WANG,[4] XUAN QUYEN DINH,[1,5] SONGNIAN FU,[4] WEIJUN TONG,[6] AND MING TANG[1,3,9]

[1]*COFT, School of EEE, Nanyang Technological University, 50 Nanyang Avenue, 639798, Singapore*
[2]*CINTRA CNRS/NTU/Thales, UMI 3288, 50 Nanyang Drive, 637553, Singapore*
[3]*College of Information Science and Engineering, Huaqiao University, Xiamen 361021, China*
[4]*National Engineering Laboratory for Next Generation Internet Access System, School of Optical and Electronic Information, Huazhong University of Science and Technology, Wuhan 430074, China*
[5]*Thales Solutions Asia Pte Ltd, R&T, 28 Changi North Rise, 498755, Singapore*
[6]*Yangtze Optical Fibre and Cable Company Ltd (YOFC), 4# Guanshan Er Road, Wuhan 430073, China*
[7]*wzh.fang@gmail.com*
[8]*epshum@ntu.edu.sg*
[9]*tangming@mail.hust.edu.cn*

Abstract: We propose and experimentally demonstrate a directional torsion sensor based on a Mach-Zehnder interferometer formed in a multicore fiber (MCF) with a ~570-μm-long helical structure (HS). The HS was fabricated into the MCF by simply pre-twisting and then heating with a CO_2 laser splicing system. This device shows the capability of directional torsion measurement from −17.094 rad/m to 15.669 rad/m with the sensitivity of ~0.118 nm/(rad/m). Moreover, since the multiple interferences respond differently to torsion and temperature simultaneously, the temperature cross-sensitivity of the proposed sensor can be eliminated effectively. Besides, the sensor owns other merits such as easy fabrication and good mechanical robustness.

OCIS codes: (060.2370) Fiber optics sensors; (060.4005) Microstructured fibers; (120.3180) Interferometry.

References and links

1. G. Wang, K. Pran, G. Sagvolden, G. B. Havsgard, A. E. Jensen, G. A. Johnson, and S. T. Vohra, "Ship hull structure monitoring using fibre optic sensors," Smart Mater. Struct. **10**(3), 472–478 (2001).
2. R. Xu, A. Yurkewich, and R. V. Patel, "Curvature, torsion, and force sensing in continuum robots using helically wrapped FBG sensors," IEEE Robot. Automat. Lett. **1**(2), 1052–1059 (2016).
3. H. M. Kim, T. H. Kim, B. Kim, and Y. Chung, "Temperature-insensitive torsion sensor with enhanced sensitivity by use of a highly birefringent photonic crystal fiber," IEEE Photonics Technol. Lett. **22**(20), 1539–1541 (2010).
4. W. G. Chen, S. Q. Lou, L. W. Wang, H. Zou, W. L. Lu, and S. S. Jian, "Highly sensitive torsion sensor based on Sagnac interferometer using side-leakage photonic crystal fiber," IEEE Photonics Technol. Lett. **23**(21), 1639–1641 (2011).
5. Y. Wang and Y. Rao, "Long period fibre grating torsion sensor measuring twist rate and determining twist direction simultaneously," Electron. Lett. **40**, 1 (2004).
6. B. Huang and X. Shu, "Ultra-compact strain- and temperature-insensitive torsion sensor based on a line-by-line inscribed phase-shifted FBG," Opt. Express **24**(16), 17670–17679 (2016).
7. N. K. Chen, J. J. Wang, G. L. Cheng, W. H. Cheng, and P. P. Shum, "Fiber torsion sensor with directional discrimination based on twist-induced circular birefringence in unbalanced Mach-Zehnder interferometer," in *CLEO: 2014*, OSA Technical Digest (online) (Optical Society of America, 2014), paper JW2A.35.
8. Q. Zhou, W. Zhang, L. Chen, T. Yan, L. Zhang, L. Wang, and B. Wang, "Fiber torsion sensor based on a twist taper in polarization-maintaining fiber," Opt. Express **23**(18), 23877–23886 (2015).
9. L. Zhang, Y. Q. Liu, X. B. Cao, and T. Y. Wang, "High sensitivity chiral long-period grating sensors written in the twisted fiber," IEEE Sens. J. **16**(11), 4253–4257 (2016).

#313596 https://doi.org/10.1364/OE.26.000544
Journal © 2018 Received 16 Nov 2017; revised 20 Dec 2017; accepted 22 Dec 2017; published 5 Jan 2018

Optics EXPRESS

10. L. Xian, P. Wang, and H. Li, "Power-interrogated and simultaneous measurement of temperature and torsion using paired helical long-period fiber gratings with opposite helicities," Opt. Express **22**(17), 20260–20267 (2014).
11. L. A. Fernandes, J. R. Grenier, J. S. Aitchison, and P. R. Herman, "Fiber optic stress-independent helical torsion sensor," Opt. Lett. **40**(4), 657–660 (2015).
12. H. Zhang, Z. Wu, P. P. Shum, X. Q. Dinh, C. W. Low, Z. Xu, R. Wang, X. Shao, S. Fu, W. Tong, and M. Tang, "Highly sensitive strain sensor based on helical structure combined with Mach-Zehnder interferometer in multicore fiber," Sci. Rep. **7**, 46633 (2017).
13. H. Zhang, Z. Wu, P. P. Shum, R. Wang, X. Q. Dinh, S. Fu, W. Tong, and M. Tang, "Fiber Bragg gratings in heterogeneous multicore fiber for directional bending sensing," J. Opt. **18**(8), 085705 (2016).
14. P. S. J. Russell, R. Beravat, and G. K. L. Wong, "Helically twisted photonic crystal fibres," Phil. Trans. R. Soc. A, in press (2017).
15. Z. L. Xu, Q. Z. Sun, J. H. Wo, Y. Dai, X. L. Li, and D. M. Liu, "Volume strain sensor based on spectra analysis of in-fiber modal interferometer," IEEE Sens. J. **13**(6), 2139–2145 (2013).
16. X. Ma, C. H. Liu, G. Chang, and A. Galvanauskas, "Angular-momentum coupled optical waves in chirally-coupled-core fibers," Opt. Express **19**(27), 26515–26528 (2011).
17. L. L. Shi, T. Zhu, Y. E. Fan, K. S. Chiang, and Y. J. Rao, "Torsion sensing with a fiber ring laser incorporating a pair of rotary long-period fiber gratings," Opt. Commun. **284**(22), 5299–5302 (2011).
18. H. Y. Choi, M. J. Kim, and B. H. Lee, "All-fiber Mach-Zehnder type interferometers formed in photonic crystal fiber," Opt. Express **15**(9), 5711–5720 (2007).
19. Y. O. Agha, F. Zolla, A. Nicolet, and S. Guenneau, "On the use of PML for the computation of leaky modes - An application to microstructured optical fibres," Compel **27**(1), 95–109 (2008).
20. Y. P. Wang, J. P. Chen, and Y. J. Rao, "Torsion characteristics of long-period fiber gratings induced by high-frequency CO_2 laser pulses," J. Opt. Soc. Am. B **22**(6), 1167–1172 (2005).

1. Introduction

Torsion is one of the most important mechanical parameters for monitoring structures and recently torsion sensors are widely used in many practical applications, for instance, structural health monitoring [1], robot position tracking [2]. Thanks to the intrinsic advantages such as compact size, easy integration, immunity to electromagnetic interference and high sensitivity, optical fiber based torsion sensors have attracted extensive research interest and have been demonstrated with different schemes such as fiber gratings or fiber interferometers. Due to the circular symmetry of normal fibers, most of fiber-based torsion sensors can only measure quantitatively the applied torsion but without the twist direction. In order to achieve the capability of twist direction discrimination, some approaches have been demonstrated to break fibers' circular symmetry. The first approach is using an asymmetric fiber as the sensing unit such as polarization-maintaining fiber (PMF) or photonics crystal fiber (PMPCF) based Sagnac interferometers [3, 4]. The second approach is using various kinds of micro-machining means to achieve the fibers' asymmetry such as fabricating a long period grating (LPG) in a single mode fiber (SMF) with a CO_2 laser [5] or a phase-shifted fiber Bragg grating (FBG) in a SMF with a femtosecond laser [6], and introducing two dissimilar abrupt tapers in a highly Er/Yb co-doped fiber [7] or a twisted taper in a PMF [8]. Another micro-machining method, fabricating helical structures (HSs) in fibers, has received considerable attention recently. For instance, a helical LPG (HLPG) [9] or paired HLPGs [10] were inscribed in SMFs by CO_2 lasers. L. A. Fernandes *et al.* proposed an interesting scheme for torsion sensor by fabricating a helical waveguide (HW) in the cladding of a SMF by a femtosecond laser [11]. The aforementioned approaches exhibited good performance, but still have some drawbacks. For example, the fabrication of PCFs is costly and relatively complicated, which are the barriers to widespread applications for PCF based torsion sensors. The conventional FBGs or LPGs normally encounter a problem of temperature cross-sensitivity [5, 9]. The fabrication of the phase shifted FBG or HW by a femtosecond laser requires ultrahigh precision and the process is complicated, because not only the laser beam needs to be precisely aligned and focused inside the fiber, but the fiber and the objective lens need to be immersed in index-matching oil [6, 11]. The taper regions result in a relatively worse mechanical strength [7, 8]. The paired HLPGs is easily affected by non-uniform external temperature perturbation due to its long length of about 60 mm [10]. Thus, an easy

Optics EXPRESS

method of fabricating a torsion sensor with twist direction discrimination and eliminating temperature cross-sensitivity is in high demand.

Recently, we have proposed and demonstrated the fabrication of HSs in a multicore fiber (MCF) by utilizing a CO_2 laser splicing system [12]. The fabrication process of the HS is easy and repeatable. In this paper, we experimentally demonstrate a torsion sensor based on a Mach-Zehnder interferometer (MZI) formed in an all-solid MCF with a HS. The length of the HS is about 570 μm, which is much shorter than that of the whole MCF. The proposed sensor can measure torsion and determine the twist direction simultaneously, and the temperature cross-sensitivity can be eliminated. In addition, the proposed sensor offers easy fabrication and has good mechanical strength due to all the segments of the sensor having the same cladding diameter and all-solid structures.

2. Configuration and principle

Figure 1(a) illustrates the cross-sectional microscope photograph of the MCF. It has six identical outer cores and one center core embedded in the pure silica cladding. The diameters of the seven cores are about 8.4 μm. The pitch, the distance between two adjacent cores, and the outer diameter are about 42 μm and 125 μm, respectively [13]. It is noteworthy that the center core was fabricated from G.652 preform while the outer cores were fabricated from G.657.B3 preform. As the measured refractive index (RI) profile shown in Fig. 1(b), each outer core has a much deeper trench surrounding the core compared with the center core. Such design combined with the relatively large pitch can inhibit the cross talk among the cores. The RI of the center core is slightly lower than that of the outer cores. In reference to the RI of the pure silica cladding, the measured RI differences of the center core, center core trench, outer cores and outer core trenches are about 0.0047, –0.0006, 0.0053 and –0.0038, respectively.

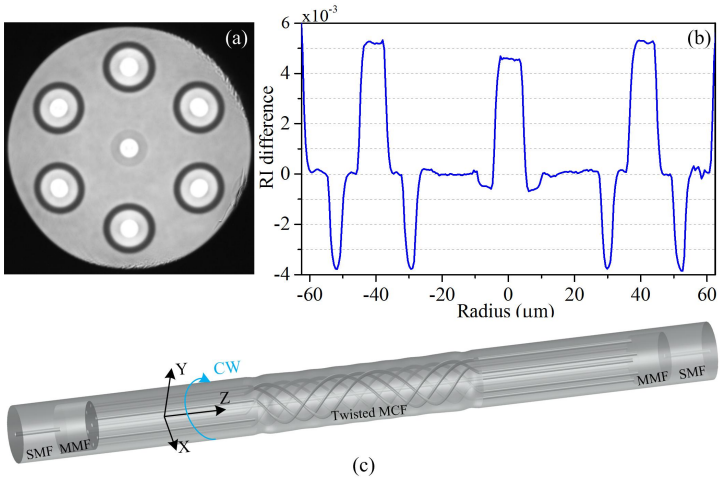

Fig. 1. (a) Cross-sectional micrograph of the MCF. (b) Measured RI profile of the MCF. (c) The schematic diagram of the sensor structure.

The configuration of the HS based sensor is depicted in Fig. 1(c). The clockwise (CW) direction is defined as the same rotational direction of the HS, as marked in Fig. 1(c). The opposite direction is defined as the counter clockwise (CCW) direction. In the HS region, the outer cores and cladding were twisted into spring shapes while the center core was almost kept straight. As a result, the effective optical path lengths, and thus the effective RIs of the outer core mode (OCM) and cladding mode (CM) were increased, while that of the center core mode (CCM) was almost kept unchanged [14]. To construct the sensor, firstly, an ultra-short HS was permanently introduced into the MCF, the description of the HS fabrication

Optics EXPRESS

method can be found in [12]. Then a segment of the MCF with the fabricated HS was connected between two multimode fibers (MMFs) via fusion splicing. The cladding and core diameters of the MMFs are 125 μm and 105 μm, respectively. Since different modes passing through the MMFs will accumulate phase differences, in order to reduce their influence on the interference spectrum of the sensor, the lengths of the MMFs should be chosen as short as possible [15]. In this work, the lengths of the MMFs were about 1 mm. At last, the sample was spliced with the lead-in and lead-out SMFs. One of the MMFs acts as a splitter coupling light from the lead-in SMF into all the seven cores and cladding, while the other one acts as a combiner coupling the light back to the lead-out SMF.

When the light propagates through the proposed structure, a series of interferences will occur among the CCM, OCM and CMs. The intensity of an interference generated by N different compositions can be expressed as:

$$I = \sum_{i=1}^{N} I_i + 2\sum_{i=1}^{N}\sum_{j=2}^{N} \sqrt{I_i I_j}\cos(\Delta\phi_{ij}), \tag{1}$$

where $i < j$, I_i and I_j present the intensities of the i-th and j-th modes, respectively. $\Delta\phi_{ij}$ denotes the phase difference between the two modes. When $\Delta\phi_{ij} = (2m+1)\pi$, where $m = 0,1,2,3...$, the destructive interference will result in the resonant dips locating at [12]:

$$\lambda_{ij} = \frac{2\left[\left(n_{eff,i} - n_{eff,j}\right)L_s + \left(n_{eff,i}^H - n_{eff,j}^H\right)L_H\right]}{2m+1}, \tag{2}$$

where $n_{eff,i}(n_{eff,i}^H)$, $n_{eff,j}(n_{eff,j}^H)$ and $L_s(L_H)$ are the refractive indices of the i-th and j-th modes, and the physically propagating lengths in the straight region (pre-twisted region), respectively.

When external torsion is applied on the fiber, photo-elastic effect will result in RI change, which can be described as $n(\tau) = n_0(1+\rho^2\tau^2)^{1/2} \approx n_0(1+\rho^2\tau^2/2)$ [14,16], where n_0 is the RI for the untwisted case, ρ is the radial distance to the center of the fiber, and τ is the twist rate (TR). In the HS region, since a permanent torsion τ_0 has been pre-induced into the fiber and caused RI change, the corresponding RI with applied torsion can be written as $n^H(\tau) \approx n_0\rho^2\left[1+(\tau\pm\tau_0)^2/2\right]$,where "+" and "–" means the applied torsion is in CW and CCW directions, respectively. As the radius of the center core is much smaller than ρ of the cladding and outer cores, the torsion induced RI change of the center core is almost zero, whereas that of the cladding and outer cores cannot be neglected [17].

According to Eq. (2), the applied torsion variation $\Delta\tau$ caused wavelength shift can be approximately expressed as:

$$\Delta_{ij} \approx \frac{2}{2m+1}\left[\frac{\delta\left(n_{eff,i} - n_{eff,j}\right)}{\delta\tau}L_s + \frac{\delta\left(n_{eff,i}^H - n_{eff,j}^H\right)}{\delta\tau}L_H\right]\Delta\tau. \tag{3}$$

For the dips λ_1 generated from the interference between the CCM and the CM, the torsion variation caused wavelength shift can be expressed as:

$$\Delta\lambda_1 \approx \frac{-2n_{eff,cl}\rho_{cl}^2\left[\tau(L_s+L_H)\pm\tau_0 L_H\right]\Delta\tau}{2m+1}, \tag{4}$$

Optics EXPRESS

where $n_{eff,cl}$ and ρ_{cl} are the effective RI and the average radius of the CM, respectively. When τ_0 is much larger than τ, the right side of Eq. (4) is mainly determined by $\tau_0 L_H$, which implies the wavelengths shift almost linearly to τ in a certain range. According to Eq. (4), the dips will shift to shorter wavelengths or longer wavelengths when the applied torsion is increased in CW direction or in CCW direction, respectively.

Similarly, for the dips generated from the interferences between the OCM and CM, the OCM and CCM, the wavelength shifts can be expressed, respectively:

$$\Delta\lambda_2 \approx \frac{2\left(n_{eff,ou}\rho_{ou}^2 - n_{eff,cl}\rho_{cl}^2\right)\left[\tau\left(L_s + L_H\right) \pm \tau_0 L_H\right]\Delta\tau}{2m+1}, \tag{5}$$

$$\Delta\lambda_3 \approx \frac{2n_{eff,ou}\rho_{ou}^2\left[\tau\left(L_s + L_H\right) \pm \tau_0 L_H\right]\Delta\tau}{2m+1}, \tag{6}$$

where $n_{eff,ou}$ and ρ_{ou} are the effective RI and the average radius distance of the outer core mode, respectively. Comparing with $\Delta\lambda_1$, $\Delta\lambda_2$ and $\Delta\lambda_3$ change in an opposite trend with varying τ. In other words, the dips generated from the interferences between the OCM and other modes, will shift to longer wavelengths or shorter wavelengths when the applied torsion is increased in CW direction or CCW direction, respectively.

3. Results and discussion

Figure 2(a) illustrates the side-view microscope photograph of the MCF with the fabricated HS. The total pre-twisted rotation angle of the HS was 4 π. As shown, only screw-type deformation was introduced into the MCF while it was still kept straight as a whole. After the HS fabrication, the sensor was fabricated according to Fig. 1(c). The lengths of the HS and the whole MCF were about 570 μm and 18.5 mm, respectively. The transmission spectrum of the sensor was measured by using a broadband light source (Infinon Research) and an optical spectrum analyzer (Yokogawa AQ6370c). Several inhomogeneous interference notches can be observed in the spectrum as shown in Fig. 2(b). By using fast Fourier transform (FFT), the corresponding spatial frequency (SF) spectrum with three strong peaks was obtained, as shown in Fig. 2(c). The three strong peaks locate at 0.0078 nm^{-1}, 0.0240 nm^{-1} and, 0.0320 nm^{-1}, respectively.

Usually, to analyze the interference compositions, the differential modal group index (DMGI) Δm can be calculated according to the SF. The DMGI of a conventional MZI without pre-twisted interference arms can be approximately derived from the SF by the following equation [18]:

$$\Delta m = \xi\lambda_0^2 / L, \tag{7}$$

where ξ, λ_0 and L denote the SF, central wavelength of the interference spectrum and whole length of the interferometer, respectively. Since the length of the whole MCF is much larger than that of the HS, Eq. (7) can be still used to roughly analyze the interference compositions of the spectrum shown in Fig. 2(b). Here λ_0 and L are 1520 nm and 18.5 mm, thus the Δm corresponding to 0.0078 nm^{-1}, 0.0240 nm^{-1} and 0.0320 nm^{-1} were calculated to be 9.7310^{-4}, 3.0310^{-3} and 4.0310^{-3}, respectively.

To further analyze the interference, the guided modes of the MCF and their corresponding effective RIs were simulated by using COMSOL Multiphysics 5.0 according to the MCF's physical parameters and RI profile. A perfect match layer (PML) was added to the outside of the cladding to absorb completely all the electric and magnetic field extending into the region [19]. The simulated mode-filed distributions of the CCM, OCM and the first order CM at

Optics EXPRESS

1520 nm are shown in Figs. 2(d)-2(f). Their effective RIs are 1.4461, 1.4466 and 1.4441, respectively. The effective RI differences between the CCM and OCM, the CCM and the first order CM, the OCM and the first order CM, are 5310^{-4}, 2.0310^{-3}, and 2.5310^{-3}, respectively.

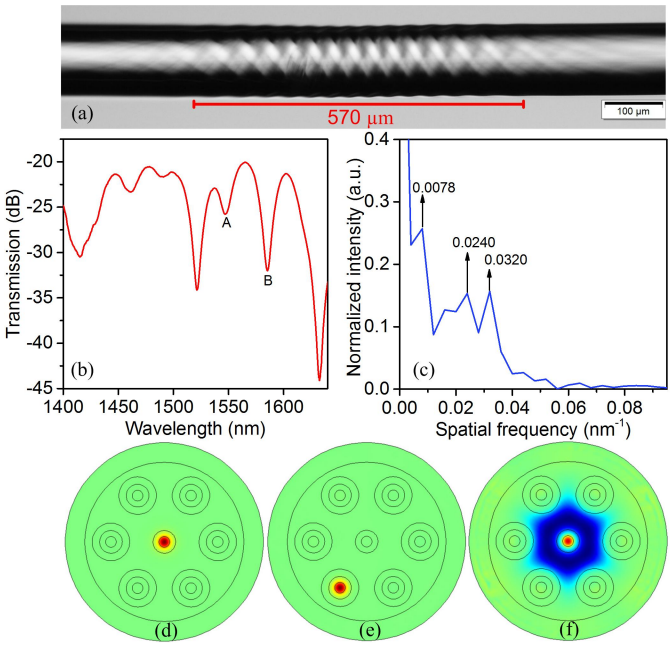

Fig. 2. (a) Side-view microscope photograph of the MCF with the fabricated HS. (b) Transmission spectrum of the proposed senor. (c) SF spectrum of the transmission spectrum. Simulated transverse mode field distribution of (d) center core mode, (e) outer core mode and (f) the first order cladding more.

Comparing the simulated effective RI differences of the supported modes with the calculated DMGIs, the fact that the peak with the SF of 0.0078 nm^{-1} should be corresponding to the interference between the CCM and OCM can be inferred. The other two peaks with the SFs of 0.0240 nm^{-1} and 0.0320 nm^{-1} could be attributed to the interferences between the CCM and CM, OCM and CM, respectively. The weak peaks observed in the SF spectrum could be mainly attributed to the higher order CMs.

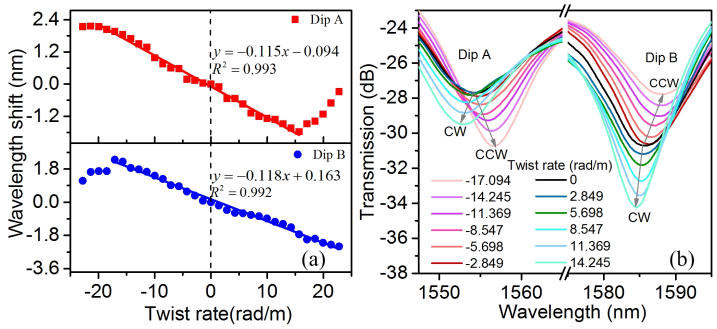

Fig. 3. (a) Wavelengths responses of Dip A and Dip B to TR. (b) Transmission spectral evolutions of Dip A and Dip B with varying TR.

In order to investigate the response to externally applied torsion, the sensor was stretched slightly and clamped between two fiber rotators (Thorlabs, PRM1/M) with a distance of about 245 mm. One rotator can be rotated in CW or CCW direction while the other one was fixed. The transmission spectra of the sensor were recorded with varying the rotation angle by a step

Optics EXPRESS

of 20 degree corresponding to a TR step of 1.4245 rad/m. The TR was increased step by step to 22.792 rad/m in CW or CCW direction. The TR value was defined as positive in CW direction while negative in CCW direction. The wavelength responses of Dip A and Dip B to TR are depicted in Fig. 3(a). As shown, when the TR was increased in CW direction, Dip A shifted linearly to shorter wavelengths for the TR up to 15.669 rad/m, and shifted back to longer wavelengths when the TR was larger than 15.669 rad/m. Different from Dip A, Dip B shifted to shorter wavelengths for the whole TR range up to 22.792 rad/m. When the TR was increased in CCW direction, both the two Dips shifted longer wavelengths firstly and then shifted back slightly. By linearly fitting the measured wavelengths, Dip A showed a torsion sensitivity of −0.115 nm/(rad/m) with the coefficient of determination (R-square) of about 0.993 within the TR range from −19.943 rad/m to 15.669 rad/m, and Dip B exhibited a torsion sensitivity of −0.118 nm/(rad/m) with R-square of about 0.992 within the TR range from −17.094 rad/m to 22.792 rad/m. As both the two dips showed blue shifts in CW direction and red shifts in CCW direction when the TR was increased, they should be generated from the interference between the CCM and CM. The two dips only showed linear responses to TR for certain TR ranges, this phenomenon should be mainly caused by the twist-induced circular birefringence in the whole fiber between the two rotators [20]. To illustrate the transmission spectral evolutions of the dips clearly, the transmission spectra according to the TR range from −17.094 rad/m to 14.245 rad/m with a step of 2.459 rad/m are shown in Fig. 3(b).

The temperature responses of the dips were also investigated. To characterize the temperature responses, the sensor was fixed in a digital-controlled oven and kept straight under slight tension. The oven has a temperature precision of 0.1 °C. The transmission spectra were measured by increasing the temperature from 30 °C to 90 °C with a step of 5 °C. Both the dips exhibited red shifts with increasing the temperature, as shown in Fig. 4(a). Figure 4(b) shows the relationships between the collected wavelengths of the two dips and the temperature variation. The temperature sensitivities of Dip A and Dip B were measured to be 0.101 nm/°C and 0.054 nm/°C by linearly fitting, respectively.

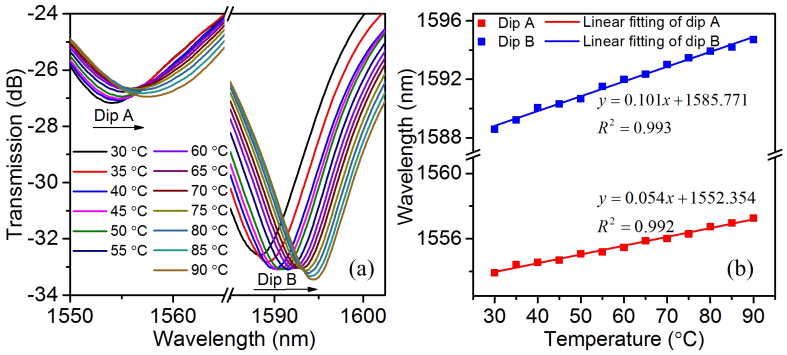

Fig. 4. (a) Transmission spectral evolutions of the two dips with temperature variation. (b) Relationships between the wavelength shift and temperature for the two dips.

The wavelength shifts of Dip A or Dip B caused by ambient temperature and applied torsion change can be expressed as:

$$\Delta\lambda_i = S_{\tau i}\Delta\tau + S_{Ti}\Delta T, (i = A, B), \tag{8}$$

where $S_{\tau i}$, S_{Ti} and ΔT represent the torsion sensitivity, temperature sensitivity, and temperature change, respectively. Since Dip A and Dip B response linearly and differently to temperature and torsion for the TR range from −17.094 rad/m to 15.669 rad/m, the torsion

Optics EXPRESS

and temperature variations can be measured simultaneously by constructing the following matrix based on Eq. (8):

$$\begin{bmatrix} \Delta\tau \\ \Delta T \end{bmatrix} = \begin{bmatrix} S_{\tau A} & S_{TA} \\ S_{\tau B} & S_{TB} \end{bmatrix}^{-1} \begin{bmatrix} \Delta\lambda_A \\ \Delta\lambda_B \end{bmatrix}. \tag{9}$$

According to the experimental results, Eq. (9) can be rewritten as:

$$\begin{bmatrix} \Delta\tau \\ \Delta T \end{bmatrix} = \begin{bmatrix} -0.115 & 0.054 \\ -0.118 & 0.101 \end{bmatrix}^{-1} \begin{bmatrix} \Delta\lambda_A \\ \Delta\lambda_B \end{bmatrix}, -17.094 \le \tau \le 15.669. \tag{10}$$

4. Conclusions

In summary, we demonstrated the fabrication of a compact helical-structure assisted Mach-Zehnder interferometer in an all-solid multicore fiber as well as its application for simultaneous measurement of directional torsion and temperature. By introducing this short helical structure, not only the fiber circular asymmetry was achieved but the multiple interference was enhanced significantly. This multiple interferences originated from the center core mode, outer core mode and cladding mode interacting each other was revealed by both FEM simulation and experimental spectrum analysis. The maximum torsion sensitivity of the proposed sensor reaches −0.118 nm/(rad/m) for the twist range from −17.094 rad/m to 15.669 rad/m. It is comparable with the sensitivity of the HLPG-based or HW-based torsion sensor [9, 11]. Although it is still lower than those of a twisted taper in a PMF [8] or paired HLPGs [10], the proposed sensor is valuable by overcoming their respective shortages as mentioned in the introduction part. Compared with the previously reported schemes utilizing micro-machining means, the proposed sensor not only owns the capability of the discrimination of directional torsion and temperature but also takes the merits of easy fabrication and good mechanical robustness.

Funding

NTU Research Scholarship; Singapore Ministry of Education Academic Research Fund Tier 2 (Grant: MOE2014-T2-1-076); Tier 1 (Grant: RG89/16); National Research Foundation Singapore (NRF) (NRF-CRP13-2014-05); Open Fund of IPOC (BUPT) and the Scientific Research Funds of Huaqiao University.